38. Ishii K, Sasaki M, Kitagaki H, Yamaji S, Sakamoto S, Matsuda K, et al. Reduction of cerebellar glucose metabolism in advanced Alzheimer's disease. J Nucl Med 1997;38:925–8.
39. Larner AJ. The cerebellum in Alzheimer's disease. Dement Geriatr Cogn Disord 1997;8:203–9.
40. Wegiel J, Wisniewski HM, Dziewiatkowski J, Badmajew E, Tarnawski M, Reisberg B, et al. Cerebellar atrophy in Alzheimer's disease-clinicopathological correlations. Brain Res 1999;818:41–50.
41. Sjöbeck M, Englund E. Alzheimer's disease and the cerebellum: a morphologic study on neuronal and glial changes. Dement Geriatr Cogn Disord 2001;12:211–8.
42. Verdile G, Gnjec A, Miklossy J, Fonte J, Veurink G, Bates K, et al. Protein markers for Alzheimer disease in the frontal cortex and cerebellum. Neurology 2004;63:1385–92.
43. Sultana R, Boyd-Kimball D, Poon HF, Cai J, Pierce WM, Klein JB, et al. Redox proteomics identification of oxidized proteins in Alzheimer's disease hippocampus and cerebellum: an approach to understand pathological and biochemical alterations in AD. Neurobiol Aging 2006;27:1564–76.
44. Chaki S, Okuyama S, Ogawa S, Tomisawa K. Regulation of NMDA-induced [$^3$H]dopamine release from rat hippocampal slices through sigma-1 binding sites. Neurochem Int 1998;33:29–34.

J Neurosurg 110:163–172, 2009

# Glioma surgery using a multimodal navigation system with integrated metabolic images

## Clinical article

Yoji Tanaka, M.D., Ph.D.,[1] Tadashi Nariai, M.D., Ph.D.,[1] Toshiya Momose, M.D.,[1] Masaru Aoyagi, M.D., Ph.D.,[1] Taketoshi Maehara, M.D., Ph.D.,[1] Toshiki Tomori, M.D.,[1] Yoshikazu Yoshino, M.D.,[1] Tsukasa Nagaoka, M.D., Ph.D.,[1,2] Kiichi Ishiwata, Ph.D.,[3] Kenji Ishii, M.D.,[3] and Kikuo Ohno, M.D., Ph.D.[1]

*[1]Department of Neurosurgery, Graduate School, Tokyo Medical and Dental University, Bunkyo-ku; [3]Positron Medical Center, Tokyo Metropolitan Institute of Gerontology, Itabashi-ku, Tokyo, Japan; and [2]Yerkes Imaging Center, Division of Neuroscience, Yerkes National Primate Center, Emory University, Atlanta, Georgia*

*Object.* A multimodal neuronavigation system using metabolic images with PET and anatomical images from MR images is described here for glioma surgery. The efficacy of the multimodal neuronavigation system was evaluated by comparing the results with that of the conventional navigation system, which routinely uses anatomical images from MR and CT imaging as guides.

*Methods.* Thirty-three patients with cerebral glioma underwent 36 operations with the aid of either a multimodal or conventional navigation system. All of the patients were preliminarily examined using PET with L-methyl-[$^{11}$C] methionine (MET) for surgical planning. Seventeen of the operations were performed with the multimodal navigation system by integrating the MET-PET images with anatomical MR images. The other 19 operations were performed using a conventional navigation system based solely on MR imaging.

*Results.* The multimodal navigation system proved to be more useful than the conventional navigation system in determining the area to be resected by providing a clearer tumor boundary, especially in cases of recurrent tumor that had lost a normal gyral pattern. The multimodal navigation system was therefore more effective than the conventional navigation system in decreasing the mass of the tumor remnant in the resectable portion. A multivariate regression analysis revealed that the multimodal navigation system–guided surgery benefited patient survival significantly more than the conventional navigation–guided surgery ($p = 0.016$, odds ratio 0.52 [95% confidence interval 0.29–0.88]).

*Conclusions.* The authors' preliminary intrainstitutional comparison between the 2 navigation systems suggested the possible premise of multimodal navigation . The multimodal navigation system using MET-PET fusion imaging is an interesting technique that may prove to be valuable in the future. *(DOI: 10.3171/2008.4.17569)*

**Key Words** • **glioma** • **magnetic resonance imaging** • **neuronavigation** • **positron emission tomography**

The infiltration of glioma cells into the functioning brain makes it difficult to aggressively resect tumors without sacrificing brain function.[8,22] Neuronavigation systems for brain tumor surgery are now widely used in daily neurosurgical practice and have been reported to improve the safety and precision of resections.[9,31] In general, these neuronavigation systems use data from MR imaging and x-ray CT scanning to help map out the brain anatomy and tumor boundaries. Although these techniques are useful for detecting even small lesions, further improvements can be made by better identification of the tumor margin. Contrast-enhanced areas on MR and CT images reflect the areas of BBB disruptions due to glioma, yet viable cells often reside beyond the areas. As a result, contrast-enhanced images sometimes fail to depict the entire margin of the tumor.[20,25] Another shortcoming of MR imaging– and CT-based navigation systems are their inability to provide information on brain function.

Among the many imaging modalities and tracers for brain tumors, MET-PET clearly detects tumor margins

*Abbreviations used in this paper:* BBB = blood-brain barrier; EBRT = external-beam radiation therapy; fMR = functional MR; MEP = motor evoked potential; MET = L-methyl-[$^{11}$C]methionine; ROI = region of interest; SSEP = somatosensory evoked potential; SUV = standardized uptake value; WHO = World Health Organization.

and accurately discerns tumor grades.[2,5,7,11,25] For this reason, the integration of MET-PET images and anatomical MR images in navigation systems is expected to provide more useful information on tumor boundaries.

Our group has long been studying the use of metabolic information with morphological information from MR imaging for the planning of glioma surgeries.[24] The aim of this study was to integrate the information from MET-PET and MR imaging into a multimodal navigation system for glioma surgery. In this manuscript, the usefulness of multimodal navigation was evaluated by comparing its findings with a conventional navigation system based solely on MR images. As we gained more experience with these techniques, we came to expect improvements in glioma resection by multimodal navigation.

## Methods

*Patient Population*

Between October 1999 and July 2005, surgeons at our institution used neuronavigation systems in 123 surgeries performed in 114 patients. Among those surgeries, 42 were performed for gliomas. In 36 of the glioma surgeries, MET-PET studies were preliminarily performed to construct PET–MR imaging fusion images for operative planning, as described in our earlier article.[24] The pathological entities were classified according to the WHO criteria as follows: 1 Grade I glioma (pilocytic astrocytoma); 7 Grade II gliomas (2 diffuse astrocytomas, 4 oligodendrogliomas, and 1 oligoastrocytoma); 16 Grade III gliomas (11 anaplastic astrocytomas and 5 anaplastic oligodendrogliomas); and 12 Grade IV gliomas (11 glioblastomas multiforme and 1 gliosarcoma). Among the 36 glioma operations, 19 were performed between June 2001 and June 2005 with a conventional navigation system based on morphological MR imaging data (Group 1, 19 cases). The other 17 glioma surgeries were performed using the multimodal navigation system between January 2003 and July 2005 by integrating multiple modalities into the navigation system (Group 2, 17 cases). Clinical data on each group are summarized in Table 1.

*Glioma Surgery*

The StealthStation (Medtronic Sofamor Danek) was used as the navigation system in all of the operations. The tumor margins in the patients in Group 2 were directly determined from the fusion images of MR imaging and MET-PET, and those in the patients in Group 1 were determined using anatomical MR images alone. The correlation between the tumor location and eloquent area was confirmed using clinical symptoms, visual inspection of anatomical MR images, results of fMR imaging, and intraoperative electrophysiological tests by using SSEP or MEP monitoring. The SSEP or MEP recording was closely monitored throughout all of the operations performed near motor eloquent areas, with the goal of achieving maximum resection without sacrificing neuronal function in all but the biopsy cases. In the biopsy cases, tissue from the tumor sections with the highest MET uptake on integrated PET images in the navigator were sampled by navigator-guided biopsy needles (Medtronic Sofamor Danek).

**Table 1: Patient characteristics in each group**

| Variable | No. of Cases | |
|---|---|---|
| | Group 1 | Group 2 |
| no. of ops | 19 | 17 |
| initial | 12 | 9 |
| reop | 7 | 8 |
| mean age (yrs) | 47.95 | 45.37 |
| sex (M/F) | 13:6 | 8:9 |
| WHO grade | | |
| I | 0 | 1 |
| II | 4 | 3 |
| III | 9 | 7 |
| IV | 6 | 6 |

The extent of resection and the success of the operation rate were evaluated based on postoperative MR imaging and MET-PET findings in all patients except for those undergoing biopsy. The patients were divided into 2 groups based on extent of resection: those who underwent total resection, in which postoperative imaging studies revealed no definitive tumor remnants; and those who underwent partial resection, in which residual tumor was recognized on either postoperative MR imaging or MET-PET imaging. All patients were examined using postoperative MR imaging. The patients in whom tumor remnants were suspected but not definitive on postoperative MR imaging underwent postoperative MET-PET (11 patients in Group 2 and 9 patients in Group 1). The presence of an apparent residual tumor was assessed by determining whether it had been decided preoperatively to leave tumor remnants in the resectable area.

*Postoperative Treatment*

Postoperative chemotherapy and fractionated EBRT were administered according to the same protocol in both groups, based on the following WHO grades and patient conditions: Grade I, no postoperative treatment was undertaken; Grade II, only fractionated EBRT was undertaken; Grades III and IV, chemotherapy and fractionated EBRT were undertaken. Gamma Knife surgery was performed for residual tumor control in the recurrent cases (6 cases in Group 2 and 7 cases in Group 1). None of the patients in either group received temozolomide as an agent during postoperative adjuvant chemotherapy because the agent had not yet been approved in Japan at the time of this study (approved in late 2006).

*Magnetic Resonance Imaging*

All MR imaging studies were performed using a 1.5-T superconducting system with a maximal gradient capacity of 25 mT/m (Magnetom Vision) and a circularly polarized head coil. The 3D anatomical MR imaging data were acquired using a turbo fast low-angle shot sequence. The imaging parameters were as follows: TR 120 msec, TE 15 msec, field of view 260 × 260 mm$^2$, matrix size

256 × 256. In total, 170 images with 1-mm contiguous sagittal slices were obtained in each patient.

Once we became technically able to do so, we began to integrate fMR images into the navigation system for the patients in Group 2 whose tumors were located proximal to the sensorimotor cortex (4 patients), to detect the sensorimotor cortex. Functional MR imaging was performed with a T2*-weighted echo planar imaging sequence (TR 0.96 second, TE 64 msec, flip angle 30°, slice thickness 5 mm, interslice gap 5 mm, field of view 260 mm, matrix 64 × 128, 5 slices), and 5 dummy imaging procedures, resulting in an acquisition time of 2 seconds for each fMR imaging volume. Each fMR imaging study consisted of 60 repetitions with 3 periods of rest and 3 periods of stimulation in alternation (in total, 65 images were obtained over 130 seconds). The motor evoked response was obtained using a finger tapping task or foot tapping task at a self-paced rate.

*Positron Emission Tomography Study With MET*

The method used for our PET study has been described previously.[24] Briefly, PET measurements were carried out by measuring the equilibrated radioactivity 20 minutes after intravenous MET injection (200–300 MBq) using a PET scanner (Headtome V, Shimadzu). The transmission data were acquired for each patient with a rotating $^{68}$Ge rod source for attenuation correction. The regional uptake of MET was expressed as an SUV calculated as (tissue activity/ml)/(injected radioisotope activity/body weight [g]), and the uptake into the tumor was expressed as the ratio of the SUV to the contralateral normal brain. The ROIs were manually placed over the tumor area on a maximum of 4 axial images to determine the SUV of the tumor. Once determined, the SUV of the ROIs was compared with the SUV of another set of ROIs in the homologous region of the contralateral normal brain.

*Image Processing and Integration*

The MR imaging and PET image integration procedure was performed using Dr. View/LINUX R2.0 software (Asahi Kasei Information Systems). Anatomical MR imaging data and MET-PET data were integrated using the automatic multimodality image registration[1] algorithm with Dr. View software. A fusion image was generated preoperatively in all patients in both groups to evaluate the tumor location and discrepancies between the MET-PET image and MR image. In Group 2, an additional fusion image was generated for use as a navigation reference during the surgery, as described later. We have previously reported that regions with a SUV/contralateral normal brain ratio of > 1.25 are very likely to bear tumors of some grade.[25] Thus, we set a tumor/contralateral normal brain ratio threshold of 1.25 to express the tumor boundary in every patient. Then, the MET-PET images were superimposed on the anatomical MR images and transferred to the navigation system for multimodal navigation. These integrated images were then used in conjunction with conventional MR images during the multimodal navigation procedure by alternately switching from one to the other.

The fMR imaging data were also analyzed with Dr. View software by the same procedure reported by Kamada et al.[13] The first 3 dummy volumes were discarded and a gaussian spatial filter (10 mm in half width) was applied for each session. Functional activation maps were calculated by cross-correlation analysis between the measured and expected activation time course for each voxel, and pixels with a z score > 3.5 were accepted. The MR images from each functional imaging session was superimposed on anatomical images using the automatic multimodality image registration algorithm and transferred to the navigation system.

*Statistical Analysis*

The rates of total resection and the rates of tumor remnants in resectable portions were compared between the 2 navigation systems by using chi-square analysis. The survival periods after the operations were compared for differences in prognosis between the groups. The Kaplan-Meier method with the log-rank test was applied for univariate analysis, and regression analysis with the Cox proportional hazard model was applied for multivariate analysis. A probability value < 0.05 was considered significant.

## Results

*Advantage of MET-PET Integrated Multimodal Navigation System*

The conventional navigation and the multimodal navigation techniques were reliably used for navigation during glioma resection via a narrow dural opening. However, the multimodal navigation technique provided more accurate information to identify the exact tumor location on a gyrus-by-gyrus basis, as verified during surgery. The multimodal navigation technique was also found to be especially useful in recurrent cases. The problem stemmed from the frequent discrepancy between the Gd-enhanced area on the T1-weighted images and the tumor location on MET-PET, and the discrepancy was usually more marked in cases with recurrent tumors.

Figure 1 shows a representative case of recurrent anaplastic oligodendroglioma. A discrepancy in distribution was seen between the Gd-enhanced area on MR imaging and the area with high uptake on MET-PET imaging. We succeeded in removing all of the tumor tissues in this patient under multimodal navigation guidance. Furthermore, pathological examination revealed tumor tissue in areas showing elevated MET uptake without showing contrast enhancement on MR imaging. Figure 2 shows another recurrent case of anaplastic astrocytoma. A previous therapy administered to this patient resulted in a loss of normal cortical structure. There was a small discrepancy in location of tumor as seen in the Gd-enhanced MR imaging images that on MET-PET. The Gd-enhanced MR image also enhances nonneoplastic granulation; hence it depicts areas that can be difficult to distinguish from tumorous tissue. This resulted in erroneous localizations when MR images were used alone, and such problems were not encountered with the multimodal navigation system due to the additional data from MET-PET. The multimodal

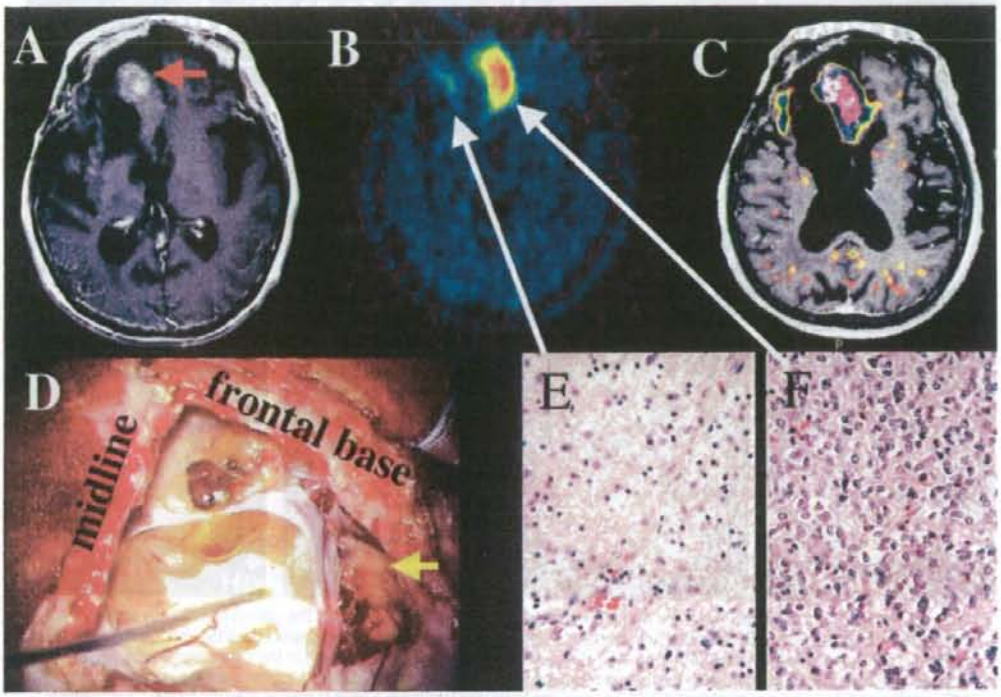


Fig. 1. Images obtained in a 72-year-old woman with recurrent anaplastic oligodendroglioma. A: Axial MR image showing a Gd-enhanced area in the medial wall of the cavity *(red arrow)*. B: An MET-PET image depicting areas of elevated uptake in the medial and lateral walls of the cavity *(white arrows)*. C and D: Comparison between the image obtained using the multimodal navigation system (C) and operative findings (D). The image created by the MR imaging–integrated multimodal navigation system reveals the area with elevated MET uptake in the lateral portion of the cavity; the texture of the cortex in this portion seemed normal (D, *yellow arrow*). E: The pathological specimen obtained from this portion actually contained tumor tissue. F: A photomicrograph of the lesion of the medial wall revealing anaplastic oligodendroglioma. According to these pathological findings, a higher MET uptake indicated higher malignancy. H & E, original magnification × 200.

navigation clearly depicted the lesions with tumorous tissue, providing adequate guidance for the excavation of the malignant astrocytoma embedded in the granulation. Total resection of the area with elevated MET uptake was confirmed by postoperative MET-PET, and the patient is, at present (4 years after the final surgery), free from lesions and symptoms.

*Comparison of Surgical Results Between Groups 1 and 2*

The surgical results in each group are summarized in Table 2. None of the patients in either group showed permanent signs of neurological deterioration or any new deficits postoperatively. Preoperative neurological deficit worsened temporarily in 3 cases from Group 1 and in 1 case from Group 2. There was no significant difference between the 2 groups regarding transient and permanent complication rate. Tumor cells were found in all of the resected tissues from all of the patients.

Total resection was achieved in 6 cases from Group 2 (1 Grade I, 1 Grade II, 3 Grade III, and 1 Grade IV glioma) and 1 case from Group 1 (1 Grade III glioma). The rate of total resection was higher in Group 2 than in Group 1, but the difference was not statistically significant ($p = 0.08$) among the operations in which maximum resection was targeted.

Maximum resection was targeted in 15 cases from Group 2 and 12 cases from Group 1. No apparent tumor remnants that had been targeted for removal were observed postoperatively in any of the patients in Group 2. In 3 cases (25%) in Group 1, unexpected tumor remnants were recognized in areas that had been preoperatively determined to be resectable. The rate of remnants in resectable portions was significantly higher in Group 1 than in Group 2 ($p = 0.02$). The tumor remnant in 1 of the 3 cases was detected by both conventional MR and MET-PET imaging, whereas those in the other 2 cases were confirmed only by MET-PET (Fig. 3). The remnant areas with high MET uptake were enhanced on the follow-up MR images in all 3 cases. These results indicated that maximal tumor removal was more accurately performed under the multimodal navigation guidance.

In 4 patients in whom the tumor was close to the mo-

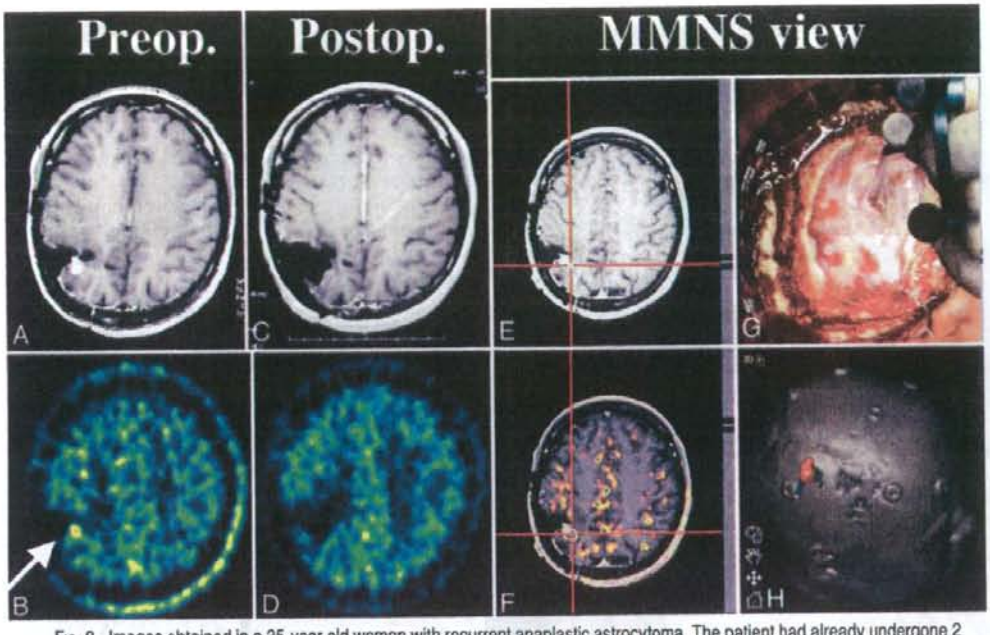


FIG. 2. Images obtained in a 35-year-old woman with recurrent anaplastic astrocytoma. The patient had already undergone 2 operations, conventional irradiation, and chemotherapy before the multimodal navigation system (MMNS)–guided removal was performed. Preoperative MR imaging (A) and MET-PET (B) showed a similar spotty lesion in the right parietal lobe *(arrow)*. In contrast, the fusion image (F) and a 3D reconstructed image (H) revealed a regional discrepancy between the enhanced spot on MR imaging and the uptake peak of the MET-PET image (the latter was located in a deeper portion than the former). Pathological examination revealed that the Gd-enhanced area mainly consisted of granulation, and that the distribution of tumor tissue corresponded closely with the area of elevated MET uptake. A covering of thickened arachnoid membrane and connective tissue over the cortical membrane resulted in a loss of the normal cortical structure (G). Regardless, the multimodal navigation system clearly depicted the lesion with elevated MET uptake (F). The patient is free from symptoms and recurrence 4 years after the operation (C and D).

tor cortex, preoperative motor mapping data with fMR imaging was integrated together with MET-PET into the multimodal navigation system. The multimodal navigation system confirmed that the area with high MET uptake was located remotely from the region activated on fMR imaging during the hand-grasping task in 3 of the 4 cases. The sensory or motor area was detected by SSEP or MEP during the operation, and the location of the sensorimotor area was compared with the area activated on fMR imaging to evaluate the accuracy of the fusion algorithms of multimodal navigation. We confirmed that the area with activated on fMR imaging corresponded closely with the sensorimotor area in all 3 cases. The area with high MET uptake was successfully resected without any deterioration of motor function in all 3 cases (Fig. 4).

### *Comparison of Patients' Outcomes Between Groups*

Eleven patients in Group 2 and 4 patients in Group 1, including 6 patients and 1 patient who underwent total removal, respectively, survived until the end of the study (February 28, 2007). The tumors resected from the patients in Group 2 were consistent with Grade I glioma in 1 case, Grade II in 3, Grade III in 5, and Grade IV in 2 cases. The tumors resected from the patients in Group 1 were consistent with 2 cases each of Grade II and III glioma.

Figure 5 shows the survival curves drawn by the Kaplan-Meier method for the groups. A statistically significant difference in the survival period was noted between the 2 groups ($p = 0.04$, log-rank test).

Correlation between the navigation system used for operation and the patient survival period was tested using a multifactorial regression analysis with the Cox proportional hazard model (Table 3). The tumor grade, patient age, purpose of surgery (radical resection vs biopsy), tumor location (frontal vs nonfrontal), and surgical timing (initial operation vs operation for recurrence) were also included as parameters in the regression model. The tumor grade was apparently the most significant determinant of survival, as expected ($p = 0.0001$). However, the multimodal navigation guidance was also found to contribute significantly to the patient survival ($p = 0.016$, odds ratio 0.52 [95% confidence interval 0.29–0.88]) compared with the conventional navigation guidance system. Younger patient age and more radical resection surgery also provided a greater benefit to prognosis ($p = 0.022$ and $p = 0.035$, respectively).

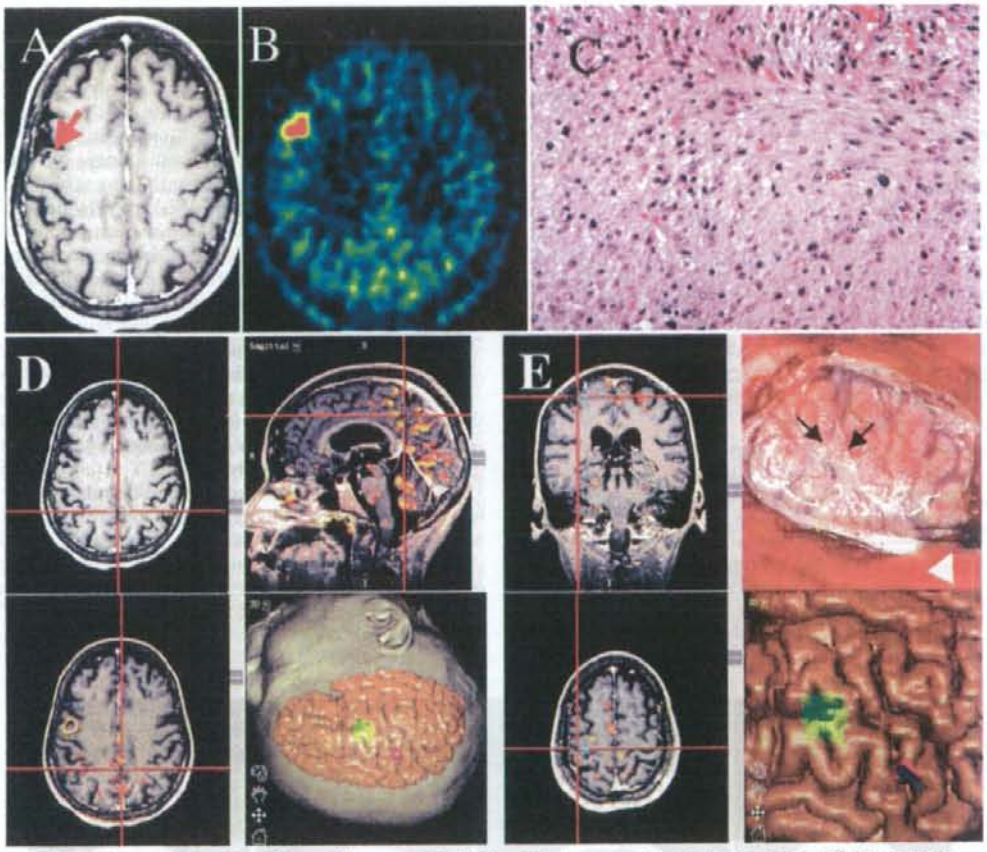


Fig. 4. Images obtained in a 59-year-old woman with right frontal lesion, presenting focal seizure in the left facial muscle. A T1-weighted MR image obtained after Gd administration (A) demonstrating a small nonenhancing lesion *(arrow)*. The MET-PET image (B) clearly delineates the tumor boundary. A photomicrograph of the lesion reveals an anaplastic astrocytoma (C). A 3D reconstructed image on multimodal navigation (D, *lower right*) clearly shows the locations of the area with elevated MET uptake *(green area)* and the area activated by hand movement task on fMR imaging *(purple area)*. The intraoperative view (E, *upper right*) corresponded closely with the 3D reconstructed image (E, *lower right*). The overlapping of the area activated by the hand motor task on fMR imaging (*blue dot* in E) and the sensorimotor cortex detected by the intraoperative electrophysiological method (SSEP and MEP using bipolar probe [*arrowhead* in E]) was confirmed. These examinations revealed that the main tumor mass in the facial motor area was located remotely from the hand motor area, and the total resection of the area with elevated MET uptake was successfully completed without causing permanent deficits (a slight dysphasia transiently appeared soon after the operation, but it disappeared within a week). H & E, original magnification × 400.

are well incorporated into viable glioma cells as a protein precursor to construct cellular components.[12] Of the various radiolabeled amino acids for PET imaging, MET is the most widely used probe in the clinical setting. Many articles have established the efficacy of MET in reflecting the viability of glioma cells and areas with tumor cell invasion.[2,5–7,11,25,28] This modality is thus expected to lead to remarkable improvements in the accuracy of glioma surgery. The use of PET scans poses a hurdle, however, in that the resolution of PET is usually too low to feasibly provide guidance for resection. As an alternative, a computer-based image registration of the PET scans to high-resolution MR imaging can provide an anatomical accuracy sufficient to perform resection on a gyrus-by-gyrus level or to enable pathological sampling. Our analysis of surgical outcome in this report justifies the use of such an image registration technique in a navigation system.

We obtained the MET-PET information in the preoperative examinations in our study even in Group 1. However these images were not incorporated into the navigation system. The discrepancy between the lesions on the MR imaging and the area with elevated uptake on the

**Table 2: Summary of surgical results in each group**

| Variable | Group 1 (19 cases) | Group 2 (17 cases) |
|---|---|---|
| op complications | | |
| temporary | 3 (15.8%) | 1 (5.9%) |
| permanent | 0 | 0 |
| tumor location | | |
| eloquent | 18 | 12 |
| noneloquent | 1 | 5 |
| resection rate | | |
| total | 1 (5.3%) | 6 (35.2%) |
| partial | 11 (57.9%) | 9 (52.9%) |
| biopsy | 7 (36.8%) | 2 (11.8%) |
| no. of ops targeting maximum resection (total + partial) | 12 | 15 |
| apparent residual tumor in resectable area | 3/12 (25%) | 0/15 (0%)* |
| detected by MRI | 1/3 | 0 |
| detected by MET-PET | 3/3 | 0 |

* Significantly less than Group 1 ($p = 0.02$).

## Discussion

A neurosurgeon must achieve 2 conflicting objectives to perform an optimal glioma surgery: to remove as much brain tissue harboring glioma cells as possible and to preserve neuronal function. To succeed, the neurosurgeon must delineate the area with glioma cell invasion in relation to the brain structure. Regrettably, the conventional navigation system does not provide sufficient information to allow this. The invasive nature of glioma and the contrast mechanism in imaging modalities such as CT and MR imaging used in the conventional navigation systems result in poor tumor delineation. Contrast-enhanced x-ray CT and MR imaging reveal areas with disruption of the BBB, but these areas seldom match the distribution of glioma cells. The T2-weighted MR images depict not only tissue with glioma cells, but also the outlying edematous tissue with high signal intensity, a tissue that tends to obscure the tumor boundary. In reports by other groups, contrast-enhanced CT[3,16] and MR imaging[20] detected tumor tissue in areas several cm away from the lesions. These findings clearly underline the need to incorporate a modality effective in revealing the glioma cell infiltration in navigation systems for glioma surgery. Radiolabeled amino acid probes used for PET imaging pass through the BBB by amino acid transporters[30] and

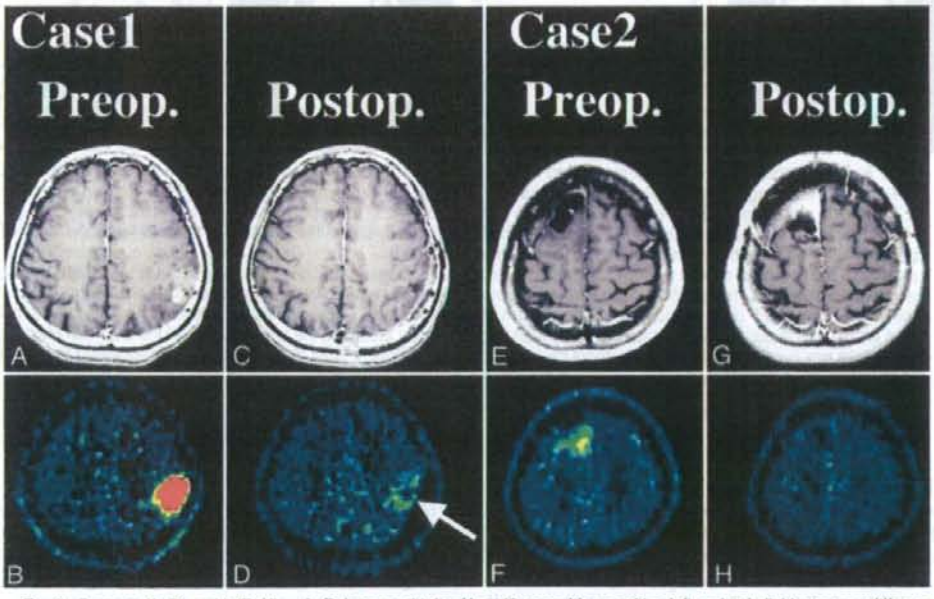


FIG. 3. Cases 1 (A–D) and 2 (E–H). A–D: Images obtained in a 40-year-old man with a left parietal glioblastoma multiforme resected using the conventional navigation system. Preoperative MR (A) and MET-PET (B) images. Postoperative MR image (C) showing total disappearance of the Gd-enhanced mass lesion, whereas the MET-PET image (D) reveals the residual lesion with elevated MET uptake *(arrow)*. E–H: Images obtained in a 38-year-old woman with a right frontal oligodendroglioma. The patient had undergone an initial surgery, with presumed total tumor removal, at another hospital. However, the MET-PET images at admission to our hospital clearly demonstrated an area with elevated MET uptake (E and F). Postoperative imaging after a second surgery using multimodal navigation revealed no evidence of remnant tumor (G and H).

**Table 3: Result of multivariate analysis with Cox proportional hazard model to analyze patients' survival after the operation (preliminary intrainstitutional comparison)***

| Factor | Odds Ratio (95% CI) | p Value |
|---|---|---|
| tumor grade | 7.83 (2.46–33.9) | 0.0001 |
| use of MMNS (vs CN) | 0.52 (0.29–0.88) | 0.016 |
| biopsy (vs resection) | 2.21 (1.05–5.38) | 0.035 |
| age | 1.04 (1.01–1.08) | 0.022 |
| op for recurrent tumor | 1.33 (0.75–2.63) | 0.337 |
| frontal lesion (vs non-frontal) | 1.69 (0.95–3.24) | 0.070 |

* CI = confidence interval; CN = conventional navigation system; MMNS = multimodal navigation system.

MET posed challenges, and it was difficult to accurately identify the areas with elevated MET uptake during surgery without directly integrating the PET image to the navigator. As it turned out, tumor remnants after surgery were detected in the resectable areas in 3 cases from Group 1. Moreover, when operating on recurrent tumors, the loss of normal cerebral surface structure and the narrowing of the opening through the dura mater by tissue adhesion make it difficult to determine the resection border based solely on preoperative planning. Enhancement with Gd may also appear in nontumorous areas as a result of other factors, such as prior treatments, granulation, and radiation injury.[21] For these reasons, we expected to obtain useful data by directly integrating the MET-PET information into the multimodal navigation system, especially in operations for recurrent tumor.

Our regression analysis in this study revealed that the multimodal navigation system provided a significant survival benefit for patients with glioma. These differences in survival could be the result of the significantly reduced number of remnants in the resectable area in multimodal navigation. Others have also pointed out the importance of complete or near-complete tumor resection for favorable outcome,[15,18] but the evaluations of the extent of residual tumor were almost always performed using conventional MR imaging. In our last report,[25] we pointed out that the differences were more clearly depicted when MET-PET was used to detect the residual tumor of malignant glioma. We therefore concluded that the integration of MET-PET into the multimodal navigation system would have a potential to improve the surgical precision, and we expect this interesting technique may prove to be valuable in the future study.

Another advantage of the multimodal navigation system is its ability to integrate a variety of metabolic and functional information. We demonstrated that fMR imaging–integrated multimodal navigation could further improve the accuracy and prognosis of the interventional procedure (Fig. 4). We are now improving the multimodal navigation system to include functional data from fMR imaging and optical imaging[23,29] as well as fiber tractography for better surgical navigation. Fiber tractography from diffusion tensor imaging is a powerful tool to provide the information about neuronal pathways that we cannot see directly.[14,19,27] Even the tumor apparently located away

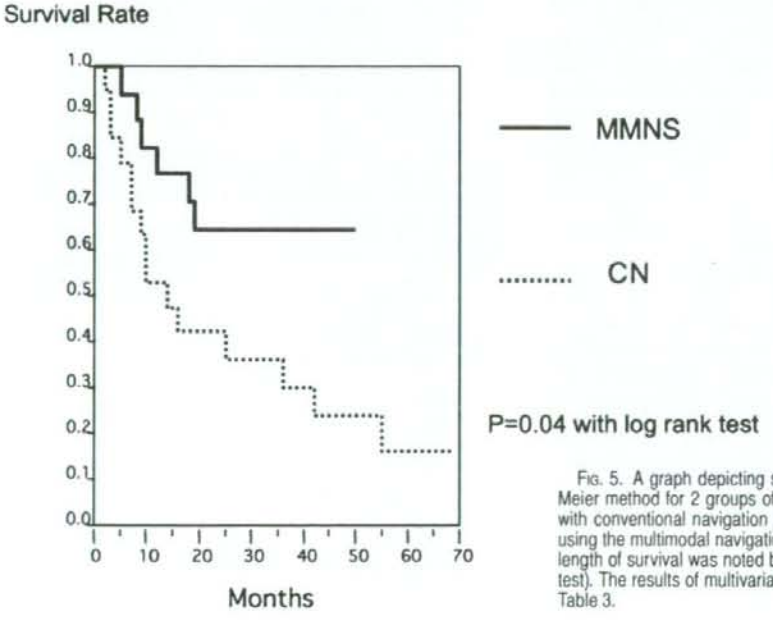


FIG. 5. A graph depicting survival curves drawn using the Kaplan-Meier method for 2 groups of patients: those who underwent surgery with conventional navigation (CN) and those who underwent surgery using the multimodal navigation system. A significant difference in the length of survival was noted between the 2 groups (p = 0.04, log-rank test). The results of multivariate regression analysis are also shown in Table 3.

from the eloquent cortex often involves some neuronal tracts, and resection without the information may cause undesirable complications. We believe that the integration of all these modalities could more accurately reveal the tumor boundary and differentiate it from functioning cerebral structures. This should significantly improve the safety and accuracy of glioma surgery in and around the eloquent cortex.

The image fusion of PET and MR imaging has already been reported by authors of several other papers, in addition to our own.[17,24,26] There has also been a report on the use of ≥ 3 modalities (PET, fMR imaging, and morphological MR imaging) in a navigation system.[2] None of these earlier reports, however, have compared the utility of the multimodal navigation system to that of a conventional navigation system, or have presented a significant difference in patient prognosis between multimodal navigation and conventional navigation groups. However, we must also note the limitation of our present comparative analysis. The present comparison was retrospectively carried out using the data acquired from a single institution. Moreover, the number of patients in either group is rather small. Therefore, the data in the present paper are preliminary results, and the statistical analysis might have been influenced by the heterogeneity of patients in each group, that is, the difference of the number of cases with tumors in noneloquent area. However, our preliminary comparison also indicated that the use of multimodal navigation is an interesting technique and has the potential in improving glioma surgery. In light of this, we think that a prospective analysis with a larger population will be necessary to confirm the usefulness of PET-based navigation.

We also expect that the benefits of multimodal navigation will become more evident when the system is used in a larger number of patients in whom malignant gliomas are detected at the earliest possible stage by MET-PET. In any case, the acceptance of MET-PET imaging as a routine clinical protocol will facilitate the beneficial use of multimodal navigation for glioma therapy. We thus eagerly await the acceptance of MET-PET, just as oncologists await [$^{18}$F]fluorodeoxyglucose-PET studies for systems in cancer therapy.[4,10]

## Conclusions

This study has demonstrated interesting techniques of a multimodal navigation system combining MET-PET images and fMR images. Further investigation with a prospective randomized analysis with large number should clarify the real benefit of multimodal navigation for patient outcome. The routine use of MET-PET studies in a daily clinical setting and multimodal navigation–guided surgery based on MET-PET findings are expected to provide robust clinical protocol for the treatment of glioma.

### Disclaimer

The authors report no conflict of interest concerning the materials or methods used in this study or the findings specified in this paper.

### References


1. Ardekani BA, Braun M, Hutton BF, Kanno I, Iida H: A fully automatic multimodality image registration algorithm. **J Comput Assist Tomogr 19:**615–623, 1995
2. Braun V, Dempf S, Tomczak R, Wunderlich A, Weller R, Richter HP: Multimodal cranial neuronavigation: direct integration of functional magnetic resonance imaging and positron emission tomography data: technical note. **Neurosurgery 48:**1178–1182, 2001
3. Burger PC, Heinz ER, Shibata T, Kleihues P: Topographic anatomy and CT correlations in the untreated glioblastoma multiforme. **J Neurosurg 68:**698–704, 1988
4. Coleman RE: Value of FDG-PET scanning in management of lung cancer. **Lancet 359:**1361–1362, 2002
5. De Witte O, Goldberg I, Wikler D, Rorive S, Damhaut P, Monclus M, et al: Positron emission tomography with injection of methionine as a prognostic factor in glioma. **J Neurosurg 95:**746–750, 2001
6. Derlon JM, Bourdet C, Bustany P, Chatel M, Theron J, Darcel F, et al: [11C]L-methionine uptake in gliomas. **Neurosurgery 25:**720–728, 1989
7. Derlon JM, Chapon F, Noel MH, Khouri S, Benali K, Petit-Taboue MC, et al: Non-invasive grading of oligodendrogliomas: correlation between in vivo metabolic pattern and histopathology. **Eur J Nucl Med 27:**778–787, 2000
8. Giese A, Westphal M: Glioma invasion in the central nervous system. **Neurosurgery 39:**235–252, 1996
9. Golfinos JG, Fitzpatrick BC, Smith LR, Spetzler RF: Clinical use of a frameless stereotactic arm: results of 325 cases. **J Neurosurg 83:**197–205, 1995
10. Gould MK, Maclean CC, Kuschner WG, Rydzak CE, Owens DK: Accuracy of positron emission tomography for diagnosis of pulmonary nodules and mass lesions: a meta-analysis. **JAMA 285:**914–924, 2001
11. Herholz K, Holzer T, Bauer B, Schroder R, Voges J, Ernestus RI, et al: 11C-methionine PET for differential diagnosis of low-grade gliomas. **Neurology 50:**1316–1322, 1998
12. Ishiwata K, Kubota K, Murakami M, Kubota R, Sasaki T, Ishii S, et al: Re-evaluation of amino acid PET studies: can the protein synthesis rates in brain and tumor tissues be measured in vivo? **J Nucl Med 34:**1936–1943, 1993
13. Kamada K, Houkin K, Iwasaki Y, Takeuchi F, Kuriki S, Mitsumori K, et al: Rapid identification of the primary motor area by using magnetic resonance axonography. **J Neurosurg 97:**558–567, 2002
14. Kamada K, Todo T, Masutani Y, Aoki S, Ino K, Takano T, et al: Combined use of tractography-integrated functional neuronavigation and direct fiber stimulation. **J Neurosurg 102:** 664–672, 2005
15. Keles GE, Chang EF, Lamborn KR, Tihan T, Chang CJ, Chang SM, et al: Volumetric extent of resection and residual contrast enhancement on initial surgery as predictors of outcome in adult patients with hemispheric anaplastic astrocytoma. **J Neurosurg 105:**34–40, 2006
16. Kelly PJ, Daumas-Duport C, Scheithauer BW, Kall BA, Kispert DB: Stereotactic histologic correlations of computed tomography- and magnetic resonance imaging-defined abnormalities in patients with glial neoplasms. **Mayo Clin Proc 62:**450–459, 1987
17. Krishnan R, Raabe A, Hattingen E, Szelényi A, Yahya H, Hermann E, et al: Functional magnetic resonance imaging-integrated neuronavigation: correlation between lesion-to-motor cortex distance and outcome. **Neurosurgery 55:**904–915, 2004
18. Lacroix M, Abi-Said D, Fourney DR, Gokaslan ZL, Shi W, DeMonte F, et al: A multivariate analysis of 416 patients with glioblastoma multiforme: prognosis, extent of resection, and survival. **J Neurosurg 95:**190–198, 2001

19. Mikuni N, Okada T, Enatsu R, Miki Y, Hanakawa T, Urayama S, et al: Clinical impact of integrated functional neuronavigation and subcortical electrical stimulation to preserve motor function during resection of brain tumors. **J Neurosurg 106:**593–598, 2007
20. Miwa K, Shinoda J, Yano H, Okumura A, Iwama T, Nakashima T, et al: Discrepancy between lesion distributions on methionine PET and MR images in patients with glioblastoma multiforme: insight from a PET and MR fusion image study. **J Neurol Neurosurg Psychiatry 75:**1457–1462, 2004
21. Moghrabi A, Tien R, Fuchs H, Longee D, McLendon R, Friedman HS: False positive images in the follow-up of patients with brain tumors. **Med Pediatr Oncol 28:**127–131, 1997
22. Nagano N, Sasaki H, Aoyagi M, Hirakawa K: Invasion of experimental rat brain tumor: early morphological changes following microinjection of C6 glioma cells. **Acta Neuropathol 86:**117–125, 1993
23. Nariai T, Sato K, Hirakawa K, Ohta Y, Tanaka Y, Ishiwata K, et al: Imaging of somatotopic representation of sensory cortex with intrinsic optical signals as guides for brain tumor surgery. **J Neurosurg 103:**414–423, 2005
24. Nariai T, Senda M, Ishii K, Maehara T, Wakabayashi S, Toyama H, et al: Three-dimensional imaging of cortical structure, function and glioma for tumor resection. **J Nucl Med 38:** 1563–1568, 1997
25. Nariai T, Tanaka Y, Wakimoto H, Aoyagi M, Tamaki M, Ishiwata K, et al: Usefulness of L-[methyl-11C] methionine-positron emission tomography as a biological monitoring tool in the treatment of glioma. **J Neurosurg 103:**498–507, 2005
26. Nimsky C, Fujita A, Ganslandt O, Von Keller B, Fahlbusch R: Volumetric assessment of glioma removal by intraoperative high-field magnetic resonance imaging. **Neurosurgery 55:** 358–371, 2004
27. Nimsky C, Ganslandt O, Fahlbusch R: Implementation of fiber tract navigation. **Neurosurgery 58 (4 Suppl):**ONS292–ONS304, 2006
28. Ribom D, Eriksson A, Hartman M, Engler H, Nilsson A, Langstrom B, et al: Positron emission tomography (11)C-methionine and survival in patients with low-grade gliomas. **Cancer 92:**1541–1549, 2001
29. Sato K, Nariai T, Tanaka Y, Maehara T, Miyakawa N, Sasaki S, et al: Functional representation of the finger and face in the human somatosensory cortex: intraoperative intrinsic optical imaging. **Neuroimage 25:**1292–1301, 2005
30. Smith QR, Momma S, Aoyagi M, Rapoport SI: Kinetics of neutral amino acid transport across the blood-brain barrier. **J Neurochem 49:**1651–1658, 1987
31. Spetzger U, Laborde G, Gilsbach JM: Frameless neuronavigation in modern neurosurgery. **Minim Invasive Neurosurg 38:**163–166, 1995

Manuscript submitted December 18, 2007.
Accepted April 24, 2008.
Please include this information when citing this paper: published online October 10, 2008; DOI: 10.3171/2008.4.17569.

Current address for Dr. Yoji Tanaka: Yerkes Imaging Center, Division of Neuroscience, Emory University, Atlanta, Georgia.
*Address correspondence to:* Tadashi Nariai, M.D., Ph.D., Department of Neurosurgery, Tokyo Medical and Dental University, 1-5-45 Yushima, Bunkyo-ku, Tokyo 113-8519 Japan. email: nariai.nsrg@tmd.ac.jp.

Ann Nucl Med (2008) 22:495–503
DOI 10.1007/s12149-008-0140-5

ORIGINAL ARTICLE

# Voxel- and ROI-based statistical analyses of PET parameters for guidance in the surgical treatment of intractable mesial temporal lobe epilepsy

**Yoshihisa Ohta · Tadashi Nariai · Kenji Ishii
Kiichi Ishiwata · Masahiro Mishina · Michio Senda
Kimiyoshi Hirakawa · Kikuo Ohno**

Received: 4 September 2007 / Accepted: 20 February 2008


**Abstract**
*Objective* Positron emission tomography (PET) can be used to locate epileptic foci in patients with mesial temporal lobe epilepsy (MTLE) by measuring multiple parameters of the brain. We investigated a series of patients with MTLE using PET measurements of three parameters: the cerebral blood flow measured with [$^{15}$O] $H_2O$, the uptake of [$^{18}$F] fluorodeoxyglucose (FDG), an index of the cerebral metabolism rate of glucose, and the distribution volume (DV) of [$^{11}$C] flumazenil (FMZ), an index of the binding potential of central benzodiazepine receptor. We compared predictive values obtained from two methods: a voxel-based statistical analysis using statistical parametric mapping (SPM) and an asymmetry index obtained by placing regions of interest (ROIs) on PET images.
*Methods* Preoperative PET data of 11 patients with surgically confirmed MTLE were retrospectively examined. In the voxel-based analysis, the PET data were analyzed using SPM99 by statistically comparing the voxel values of PET parameters between individual patients and the mean values of 12 normal volunteers. Voxels with values significantly lower than the normal control values were mapped on a standard brain atlas. In the ROI-based analysis, the asymmetry index was calculated to depict ROIs with abnormally decreased values when compared with the contralateral side.
*Results* (1) Statistical parametric mapping and ROI analyses of the FDG uptake correctly determined epileptic temporal lobe in 73% and 82%, respectively. (2) The decreased DV of FMZ depicted by SPM revealed the mesial temporal pathology in 91%.
*Conclusions* Positron emission tomography measurement of FDG uptake was most sensitive in detecting the side of the epileptic focus. On the other hand, SPM analysis of the DV of FMZ was the most sensitive method for delineating the actual epileptic focus.

**Keywords** Mesial temporal lobe epilepsy · Presurgical evaluation · Positron emission tomography · Fluorodeoxyglucose · Central benzodiazepine receptor

Y. Ohta · T. Nariai (✉) · K. Hirakawa · K. Ohno
Department of Neurosurgery, Tokyo Medical and Dental University, 1-5-45 Yushima, Bunkyo-ku, Tokyo 113-8519, Japan
e-mail: nariai.nsrg@tmd.ac.jp

K. Ishii · K. Ishiwata · M. Mishina · M. Senda
Positron Medical Center, Tokyo Metropolitan Institute of Gerontology, Tokyo, Japan

M. Mishina
Department of Neurology, Nippon Medical School Chiba Hokusoh Hospital, Chiba, Japan

M. Senda
Department of Image-based Medicine, Institute of Biomedical Research and Innovation, Kobe, Japan

## Introduction

An accurate localization of the epileptic focus is essential to achieve optimal results in epilepsy surgery. The epileptic focus is assessed presurgically using multimodal evaluation methods such as interictal and ictal scalp electroencephalography, computed tomography, magnetic resonance imaging (MRI), positron emission tomography (PET), and the depiction of seizure patterns. Of these, the PET imaging modality measures multiple parameters non-invasively to depict functional changes of the brain which complement the structural changes

depicted by MRI, such as abnormal intensity or configuration of the hippocampus [1, 2]. Measurements of regional indicators for cerebral blood flow (CBF), the uptake of fluorodeoxyglucose (FDG), an index of the cerebral metabolism rate of glucose (CMRglc), and the distribution volume (DV) of [$^{11}$C] flumazenil (FMZ), an index of the binding potential of central benzodiazepine receptor (cBZR), are helpful for localizing the epileptic focus [1–6]. Earlier studies have sought to elucidate the differences between these three parameters in one-on-one comparisons. One study compared CBF with CMRglc [7–9], for example, and another compared CMRglc with the binding potential of cBZR [10, 11]. No studies, however, have attempted simultaneous comparisons among all the three.

Visual interpretation is widely applied as a subjective method for assessing PET images in clinical practice. One of the principle methods for objective assessment is to sample radioactivity with regions of interest (ROIs). An ROI analysis can evaluate an abnormal area by sampling the activity itself or by comparing the right and left structures. The newly developed technique of statistical parametric mapping (SPM) applies voxel-based statistical analyses for the assessment of neuroimages. SPM is automatic and absolutely user independent. However, given the breadth of the analytical methods to choose from, the conclusions they provide may well differ.

In this study, we investigated the predictive value of PET measurements of CBF, FDG uptake, and DV of FMZ in mesial temporal lobe epilepsy (MTLE) patients with surgically confirmed epileptic foci in the mesial temporal lobe. We compared the results obtained by two objective analytical methods: voxel-based statistical analysis using SPM and an ROI-based analysis using calculations of asymmetry indexes. We sought to show which PET parameters and which analytical methods offered the most useful information to depict accurately the epileptic focus and to optimize the surgical outcome in MTLE.

## Materials and methods

### Subjects

Pretreatment data of 11 consecutive patients who had been diagnosed with intractable MTLE and surgically treated at our institution (six women and five men; mean age 32.5 years; range 18–45 years) were retrospectively evaluated. The epileptic focus was localized prior to the operations using the following standard techniques for preoperative evaluation: monitoring of the seizure pattern, neuropsychological studies, interictal and ictal electroencephalography (including sphenoidal leads), intracranial electrocorticography (in eight patients only), and MRI and PET measurements of CBF, FDG uptake, and the DV of FMZ. All the patients underwent anterior temporal lobectomy (left eight and right three) following the determination of the operative side by the multimodal presurgical evaluations described earlier, including visual PET assessments. Resection was extended to the middle and inferior temporal gyri (3–5 cm), amygdala, fusiform gyri, parahippocampal gyri, and hippocampi (3–3.5 cm). The mean follow-up period following surgery was 3.55 years (2.0–5.5 years). According to the classification of seizure outcome by Engel's system [12], eight patients achieved class 1 (seizure free) and three achieved class 3 (worthwhile improvement). These results confirmed that the epileptic focus of each patient was included in the area resected. The case profile is summarized in Table 1.

Five normal volunteers (mean 22.6 years, range 22–23 years) with no history of neurological disease were recruited as controls for the CBF and FMZ data analysis, and another seven (mean 32.4 years, range 24–51 years) were recruited for the FDG uptake analysis.

The local ethical committee of Tokyo Metropolitan Institute of Gerontology approved this clinical protocol. All the participants provided their written informed consent on consent forms with clear explanations of the object of the measurements, the duration of the study,

**Table 1** Case profile

| No. | Age/sex | Side determined by ECoG | Side of resected temporal lobe | Outcome (Engel's grade) |
|---|---|---|---|---|
| 1 | 18/F | rt | rt | 1 |
| 2 | 45/M | rt | rt | 1 |
| 3 | 36/M | rt | rt | 1 |
| 4 | 33/F | lt | lt | 1 |
| 5 | 21/F | lt | lt | 1 |
| 6 | 34/F | lt | lt | 1 |
| 7 | 38/M | ND | lt | 1 |
| 8 | 38/F | ND | lt | 1 |
| 9 | 26/M | lt | lt | 3 |
| 10 | 36/F | lt | lt | 3 |
| 11 | 33/M | ND | lt | 3 |

*ECoG* electrocorticography, *ND* not done

the amount of radiation exposure, and the amount of blood sampling.

## PET methodology

The PET studies were performed with a Headtome-IV scanner (Shimadzu, Kyoto, Japan) set to provide 14 axial tomographic images with center-to-center intervals of 6.5 mm. The PET images after reconstruction had a spatial resolution of $7.5 \times 7.5 \times 9.0$ mm full width at half maximum (FWHM). Attenuation correction was performed by transmission scan with a $^{68}Ga/^{68}Ge$ source. CBF was measured by administering a bolus injection of 1 GBq of [$^{15}O$] $H_2O$ and assessing the brain by PET autoradiography with continuous arterial blood sampling. FDG uptake was measured by a 12-min static scan performed 45 min after an intravenous injection of 150 MBq of [$^{18}F$] FDG. The [$^{18}F$] FDG uptake was evaluated as a standardized uptake value on the basis of a regional radioactivity normalized by the injected dose and body weight. The cBZR binding potential was measured by injecting 500 MBq of [$^{11}C$] FMZ intravenously and performing a dynamic scan and serial arterial blood sampling for 60 min. The DV of FMZ was calculated on the basis of a two-compartment model and expressed as a pixel-by-pixel parametric image.

## Statistical analysis of PET parameters

### *Voxel-based analysis*

Image manipulations were carried out on an Indy workstation (Silicon Graphics, Mountain View, CA, USA) using SPM99 (Wellcome Department of Cognitive Neurology, Institute of Neurology, London, UK) software. The PET data of each patient were statistically compared with those of normal volunteers. The CBF data were normalized with a 12-parameter affine transformation using a CBF template from SPM99. The FDG uptake data were normalized with a 12-parameter affine transformation using an FDG template devised by a multicenter study in Japan. Data on the DV of FMZ were registered on their own MRI using an automated image registration program (AMIR) [13]. MR-registered FMZ-DV data were normalized with a 12-parameter affine transformation using an MR T1 image template from SPM99. The PET data were smoothed with a Gaussian kernel of 15 mm FWHM. The areas with abnormally decreased distributions of CBF, FDG uptake, and FMZ-DV were mapped with a $P < 0.05$ threshold without correction for multiple comparisons. The assessments were based on three axial slices, which are the slices at $Z = -24, -18, -12$ of Talairach's standard brain. The side of the epileptic temporal lobe was determined by two authors (YO and TN) independently. The authors individually studied the distribution maps to evaluate whether the temporal lobe possessed an abnormal area. The temporal lobe with a greater number of abnormal pixels was assessed as epileptic. When abnormal pixels were distributed on both sides equally, they were determined to be "equally distributed" cases. When abnormal pixels were not depicted in either temporal lobe, the cases were determined to be "not detected" cases. When the two investigators arrived at the same result, the result was determined as the final judgment. When their results were discordant, the cases were concluded to be "equally distributed" cases.

### *ROI-based analysis*

Image manipulations were carried out on an Indy workstation with Dr. View; medical image-processing software (Asahi Kasei Joho System, Tokyo, Japan). PET data of each patient were co-registered to their own MRI using AMIR. Coronal PET and MRI parallel to the floor of the fourth ventricle [14] were re-sliced from the original axial image at 5 mm intervals. Circular ROIs were manually placed on the temporal lobe over the MRI (Fig. 1). The ROIs on the mesial temporal structure and lateral temporal lobe were 0.5 cm and 1.0 cm in diameter, respectively. The ROIs with significantly greater reductions in parameter values compared with the contralateral side were determined by calculating the asymmetry index ($AI = (lt - rt) \times 2/(lt + rt)$) for each patient and normal control subject. When the AI of a patient was outside the mean ± SD range of that in normal controls, the ROI was determined to have an abnormally decreased value on either side.

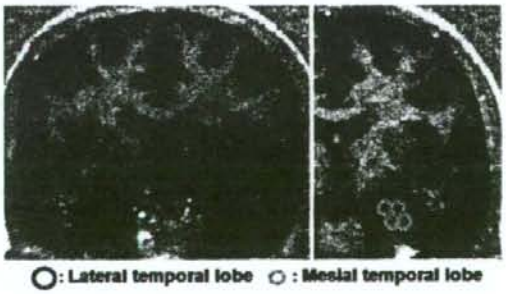


**Fig. 1** The method used to manually place regions of interest (ROIs) on the mesial and lateral temporal lobes is indicated. Circular ROIs were placed on the coronal image of patient magnetic resonance imaging (MRI). The positron emission tomography (PET) data on the ROIs were obtained by co-registering the ROIs on MRI using an automated image registration program


**Fig. 2** The results of a voxel-based statistical image analysis using statistical parametric mapping are displayed using three representative axial slices of magnetic resonance images ($Z = -24, -18, -12$) conforming to the shape of Talairach's standard brain. Voxels with statistically significant decreases of cerebral blood flow (*CBF*), fluorodeoxyglucose (*FDG*) uptake, and distribution volume of flumazenil (*FMZ*) in comparison with the levels in normal control volunteers are displayed for all 11 patients. Statistical significance was set as $P < 0.05$ without correction for multiple comparisons

## Results

### Determination of the side of the epileptic temporal lobe

The first step was to determine the side of the epileptic temporal lobe. According to the SPM analysis as shown in Fig. 2, the CBF-PET study depicted a more widely distributed abnormal area in the epileptic temporal lobe than in the contralateral side in three (27.3%) patients. The FDG uptake and FMZ-DV depicted a more widely distributed abnormal area in the epileptic temporal lobe in eight (72.7%) and six (54.5%) patients, respectively. According to the ROI-based analysis, the CBF-PET study depicted the epileptic temporal lobe in four (36.4%) patients. The FDG uptake and FMZ-DV depicted it in nine (81.8%) and seven (63.6%) patients, respectively. Results are summarized in Table 2 and Fig. 3.

### Determination of the side of the epileptic mesial temporal lobe

According to the SPM analysis, the CBF, FDG uptake, and FMZ-DV correctly determined the laterality of the

**Table 2** Determination of the side of the epileptic temporal lobe

| No. | Side of epileptic focus | CBF | | FDG | | FMZ | |
|---|---|---|---|---|---|---|---|
| | | SPM | AI | SPM | AI | SPM | AI |
| 1 | rt | rt = lt(ED) | −0.02717 | **rt** | **0.17179** | **rt > lt** | **0.06868** |
| 2 | rt | **rt** | **0.10281** | **rt** | **0.16715** | **rt** | **0.09767** |
| 3 | rt | **rt** | **0.09345** | **rt** | **0.13493** | **rt** | **0.04648** |
| 4 | lt | ND | **−0.06737** | **lt** | **−0.13231** | rt = lt(ED) | **−0.03159** |
| 5 | lt | *rt* | *0.05733* | *rt > lt* | −0.00598 | *rt* | 0.01002 |
| 6 | lt | *rt > lt* | *0.15379* | *rt > lt* | *0.10736* | rt = lt(ED) | *0.04062* |
| 7 | lt | ND | 0.02721 | **rt < lt** | **−0.06075** | **rt < lt** | **−0.03742** |
| 8 | lt | rt = lt(ED) | −0.02118 | **rt < lt** | **−0.07488** | rt = lt(ED) | **−0.01725** |
| 9 | lt | **lt** | **−0.17666** | **rt < lt** | **−0.21805** | **rt < lt** | −0.00371 |
| 10 | lt | rt = lt(ED) | *0.10548* | **rt < lt** | **−0.11890** | rt = lt(ED) | **−0.01199** |
| 11 | lt | ND | 0.03349 | rt = lt(ED) | **−0.04820** | **lt** | 0.03488 |
| AI of Normal controls | | | | | | | |
| | *n* | | 5 | | 7 | | 5 |
| | Mean | | −0.00940 | | 0.00970 | | 0.01620 |
| | SD | | 0.05400 | | 0.04970 | | 0.02050 |
| Correct lateralized | | 3 | 4 | 8 | 9 | 6 | 7 |
| Not lateralized (ND + ED) | | 6 (3 + 3) | 4 | 1 (0 + 1) | 1 | 4 (0 + 4) | 3 |
| False lateralized | | 2 | 3 | 2 | 1 | 1 | 1 |

*Bold type* indicates correctly lateralized; *italic type* indicates falsely lateralized
*CBF* cerebral blood flow, *FDG* fluorodeoxyglucose, *FMZ* flumazenil, *SPM* statistical parametric mapping, *AI* asymmetry index, *ND* not detected, *ED* equally distributed, *rt > (or <) lt* bilaterally distributed but right (or left) side bore more abnormal voxels than left (or right), *rt = lt (ED)* bilaterally equally distributed

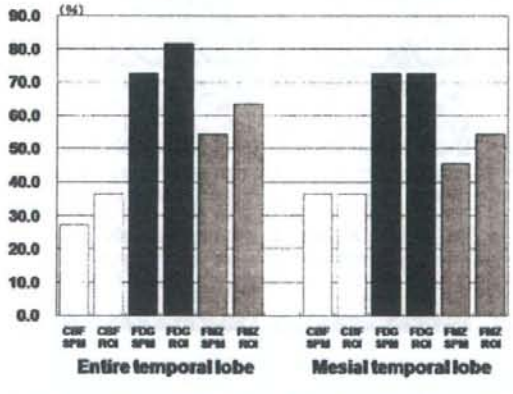


**Fig. 3** The predictive value of the side of epileptic temporal lobe. The ratios of correct lateralization determined with data on the entire temporal lobe are displayed on the *left*. The ratios determined with data on the mesial temporal structure are displayed on the *right*. The uptake of *FDG* was the most efficient parameter for determining the laterality of the epileptic focus. Statistical parametric mapping (*SPM*) analysis predicted the laterality as precisely as the ROI analysis. As the graph shows, the same degree of laterality was detected under two conditions: when the entire temporal lobe was investigated and when only the mesial temporal structure was investigated. The analysis of *FMZ-PET* was the second most sensitive method for the SPM and ROI analyses. Cerbral blood flow (*CBF*) measurement was not a sensitive method by either analysis

epileptic focus on the mesial temporal structure in four (36.4%), eight (72.7%), and five (45.5%) patients, respectively. According to the ROI-based analysis, the CBF, FDG uptake, and FMZ-DV correctly determined the laterality in four (36.4%), eight (72.7%), and six (54.5%) patients, respectively. Results are summarized in Table 3 and Fig. 3.

### Detection of mesial temporal pathology

The next analyses sought to determine whether each study could depict the epileptic mesial temporal structure as abnormal. According to the SPM analysis, the CBF, FDG uptake, and FMZ-DV depicted the existence of mesial temporal abnormality in seven (63.6%), eight (72.7%), and ten (90.9%) patients, respectively. According to the ROI analysis, these studies depicted the existence of mesial temporal abnormality in four (36.4%), eight (72.7%), and six (54.5%) patients. Results are summarized in Table 4 and Fig. 4.

## Discussion

Positron emission tomography was used to measure three parameters in patients with MTLE: the CBF, the uptake of FDG, an index of the CMRglc, and the DV of [$^{11}C$] FMZ, an index of the binding potential of cBZR.

**Table 3** Determination of the side of the epileptic mesial temporal lobe

| No. | Side of epileptic focus | CBF | | FDG | | FMZ | |
|---|---|---|---|---|---|---|---|
| | | SPM | AI | SPM | AI | SPM | AI |
| 1 | rt | **rt > lt** | 0.01598 | **rt** | **0.14749** | **rt** | **0.22633** |
| 2 | rt | **rt** | **0.07343** | **rt** | **0.22365** | **rt** | **0.33144** |
| 3 | rt | **rt** | **0.10638** | ND | **0.06273** | **rt** | **0.05703** |
| 4 | lt | ND | −0.03333 | **lt** | **−0.14768** | rt = lt(ED) | 0.01055 |
| 5 | lt | *rt* | −0.00412 | **lt** | **−0.05893** | *rt* | 0.04483 |
| 6 | lt | rt = lt(ED) | *0.09687* | ND | *0.18400* | rt = lt(ED) | 0.05144 |
| 7 | lt | ND | *0.15979* | *rt* | 0.00905 | rt = lt(ED) | 0.00835 |
| 8 | lt | rt = lt(ED) | **−0.14384** | **lt** | **−0.10418** | rt = lt(ED) | **−0.15056** |
| 9 | lt | **lt** | **−0.29596** | **lt** | **−0.22924** | **rt < lt** | **−0.09613** |
| 10 | lt | *rt > lt* | *0.11259* | **lt** | −0.02080 | rt = lt(ED) | **−0.07084** |
| 11 | lt | ND | −0.03444 | **lt** | **−0.07460** | **lt** | −0.00028 |
| AI of Normal controls | | | | | | | |
| | *n* | | 5 | | 7 | | 5 |
| | Mean | | −0.01240 | | −0.01646 | | 0.00709 |
| | SD | | 0.07906 | | 0.03818 | | 0.04486 |
| Correctly lateralized | | 4 | 4 | 8 | 8 | 5 | 6 |
| Not lateralized (ND + ED) | | 5 (3 + 2) | 4 | 2 (2 + 0) | 2 | 5 (0 + 5) | 5 |
| Falsely lateralized | | 2 | 3 | 1 | 1 | 1 | 0 |

*Bold type* indicates correctly lateralized; *italic type* indicates falsely lateralized

**Table 4** Detection of mesial temporal pathology

| No. | Side of epileptic focus | CBF | | FDG | | FMZ | |
|---|---|---|---|---|---|---|---|
| | | SPM | AI | SPM | AI | SPM | AI |
| 1 | rt | **rt > lt** | 0.01598 | **rt** | **0.14749** | **rt** | **0.22633** |
| 2 | rt | **rt** | **0.07343** | **rt** | **0.22365** | **rt** | **0.33144** |
| 3 | rt | **rt** | **0.10638** | ND | **0.06273** | **rt** | **0.05703** |
| 4 | lt | ND | −0.03333 | **lt** | **−0.14768** | **rt = lt(ED)** | 0.01055 |
| 5 | lt | rt | −0.00412 | **lt** | **−0.05893** | rt | 0.04483 |
| 6 | lt | **rt = lt(ED)** | 0.09687 | ND | 0.18400 | **rt = lt(ED)** | 0.05144 |
| 7 | lt | ND | 0.15979 | rt | 0.00905 | **rt = lt(ED)** | 0.00835 |
| 8 | lt | **rt = lt(ED)** | **−0.14384** | **lt** | **−0.10418** | **rt = lt(ED)** | **−0.15056** |
| 9 | lt | **lt** | **−0.29596** | **lt** | **−0.22924** | **rt < lt** | **−0.09613** |
| 10 | lt | **rt > lt** | 0.11259 | **lt** | −0.02080 | **rt = lt(ED)** | **−0.07084** |
| 11 | lt | ND | −0.03444 | **lt** | **−0.07460** | **lt** | −0.00028 |
| AI of Normal controls | | | | | | | |
| | *n* | | 5 | | 7 | | 5 |
| | Mean | | −0.01240 | | −0.01646 | | 0.00709 |
| | SD | | 0.07906 | | 0.03818 | | 0.04486 |
| Detected | | 7 | 4 | 8 | 8 | 10 | 6 |

*Bold type* indicates detection of the epileptic mesial temporal structure

All the three of these parameters are widely applied as preoperative evaluations for epilepsy surgery. In this study, we compared the predictive values of these parameters simultaneously in the MTLE patients enrolled. To our knowledge, this was the first study to attempt this. Our aim was to identify which parameter was most effective for determining the side of the epileptic temporal lobe in the preoperative evaluation of MTLE.

In addition to comparing PET parameters, we studied the difference between predictive values obtained by two objective analytical methods, namely, SPM and an asymmetry index analysis performed using an ROI-based method.

Statistical parametric mapping is a completely automatic, user-independent, and objective voxel-based method that can be performed without relying on predefined ROIs. In this study, we used SPM analysis to lateralize the epileptic focus by determining which side of the temporal lobe had a significantly larger number of abnormal pixels when compared with the contra-

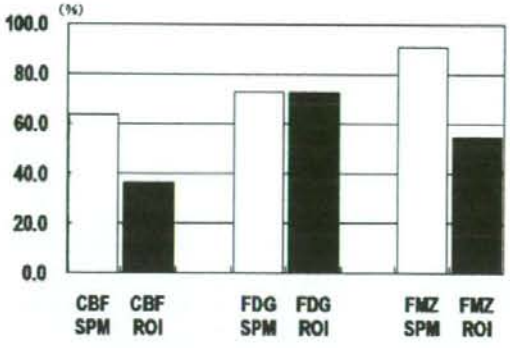


Fig. 4 The detectability of the mesial temporal pathology using three PET ligands and two analysis methods. The graph shows the ratios indicative of abnormality on the resected epileptic mesial temporal structure. Analysis of *FMZ-PET* by *SPM* detected the mesial temporal pathology most precisely

lateral side. Widespread hypometabolism has been attributed to additional epileptogenic areas, the effects of diaschisis, seizure propagation sites via anatomic network, and secondary epileptogenic foci, and has a confirmed association with the epileptogenicity [15, 16]. In light of this, we conjectured that the temporal lobe with the larger number of abnormal pixels was more closely related to the epileptogenicity and that the side of the epileptic focus could be reliably determined on the basis of the expanse of the abnormal area on the temporal lobe.

Anterior temporal lobectomy controlled the epileptic seizures in every case, thereby surgically confirming the side of the epileptic focus. Surgical validation is the golden standard for determining the epileptic focus. In light of this, the utility of PET as a presurgical evaluation should be discussed on the basis of surgically validated cases.

Epileptic foci are generally depicted as areas of interictal hypoperfusion by CBF studies. The CBF sometimes remains normal in all cerebral regions, however, or complex patterns of regional hypoperfusion are sometimes seen. As an added difficulty, interictal hypoperfusion occasionally occurs predominantly contralateral to the epileptic temporal lobe. Some have argued that these inconsistencies rule out CBF imaging as a useful clinical modality for presurgical evaluation [3]. According to the SPM and ROI analyses in our study, an interictal CBF objective study predicted the side of the epileptic temporal lobe in 27.3% (3/11) and 36.4% (4/11) of the subjects, respectively. The interictal CBF-PET study apparently lacks the efficiency required to determine the side of the epileptic temporal lobe.

The glucose metabolism of the epileptic temporal lobe decreases in 70–90% of MTLE cases [2, 3]. According to evaluations by the asymmetry index, FDG-PET studies have predictive values of 69–90% in surgically validated cases of MTLE [17–19]. Interictal FDG-PET has thus been widely applied to presurgical protocols for epileptic foci, and its performance has been reliable. The SPM analysis in our study indicated that the resected temporal lobes of 72.7% (8/11) of the cases had more voxels with significantly reduced FDG uptake when compared with the contralateral side. The ROI analysis, meanwhile, lateralized the correct temporal lobe in 81.8% (9/11) of the cases. The side of the epileptic temporal lobe determined using SPM in all the correctly lateralized cases was consistent with that determined by ROI analysis. These results support two conclusions: first, that FDG uptake measurement by PET is very effective for determining the side of the epileptic temporal lobe; second, that SPM analysis predicts the side of the temporal lobe as reliably as ROI analysis. ROI analysis is a standard method to lateralize the epileptic focus of patients with MTLE. The method can be challenging to apply, however, because experts with experience and knowledge have to place ROIs to ensure a reliable analysis. SPM analysis, on the other hand, can automatically provide an objective statistical map that can be visually interpreted as a substitute for ROI analysis. Thus, SPM analysis is easier to apply than ROI analysis for daily clinical decisions once a normal image database and a digital image transfer system are established.

A decreased binding potential of cBZR demonstrated by FMZ-PET imaging was confirmed to represent the ictal onset zone in several PET studies. The predictive values of subjective analyses using an asymmetry index reached 93–100% in surgically validated cases of MTLE [20–23]. In contrast, SPM and ROI analyses correctly identified the side of the focus in only 54.5% (6/11) and 63.6% (7/11) of our patients, respectively. The area with significantly decreased DV of FMZ was detected in bilateral mesial temporal structures in most of our cases, as shown in Fig. 2. We attributed the poor predictive value of FMZ imaging to this bilateral involvement.

The detectability of true epileptic foci is another point for discussion. The onset of the mesial temporal seizure was confirmed by either intracranial electrocorticography or surgical results in all of our subjects. Glucose hypometabolism has been reported to take on a more severe appearance in the lateral temporal lobe than in the mesial structure, and abnormal findings on the mesial temporal lobe are difficult to depict definitively even in MTLE [3]. In contrast, our studies detected the significant laterality of FDG uptake and the voxels with abnormally decreased FDG uptake in the mesial tempo-

ral structure. This information was useful to determine the side of the epileptic focus.

When we tried to estimate whether the epileptic origin was the mesial or lateral structure, however, the FDG data did not lead us to a correct answer. Most of the voxels with significantly reduced FDG uptake were located among the lateral temporal structures, as indicated in Fig. 2. On the other hand when we surveyed using SPM analysis, the significant reduction in FMZ-DV indicated that the epileptic focus was in the mesial temporal structure and not in the lateral structure.

The epileptic focus of MTLE is known as hippocampal sclerosis, i.e., neuronal cell loss in the hippocampus. The cBZR resides in neuronal cells, and neuronal cell loss leads to a decrease of the cBZR binding potential. Thus, a decrease in cBZR binding potential implies pathological changes such as hippocampal sclerosis. As mentioned earlier, our SPM analysis identified bilateral mesial temporal abnormality in six (54.5%) of our cases. This confirmed bilateral hippocampal sclerosis, a condition reported in 50–86% of cases with MTLE [24]. A recent volumetric study using MRI revealed significant volume reductions of mesial temporal structures contralateral to regions of hippocampal atrophy even in unilateral MTLE [25]. This bilateral mesial temporal damage in MTLE leads to bilateral decreases in FMZ-DV and poor sensitivity of the lateralization of the epileptic focus as a consequence. To clarify the significance of bilateral abnormality of the hippocampus, further analysis to compare the FMZ-DV in mesial temporal lobe with the degree of changes in MR parameters, such as high intensity or abnormal configuration of hippocampus, may be useful.

The crucial target in preoperative evaluation for MTLE is to determine the side of the epileptic temporal lobe. Our study confirmed that CMRglc was the most useful PET parameter to lateralize the epileptic temporal lobe. On the other hand, our SPM analysis of FMZ-PET depicted the mesial temporal pathology most clearly and was sensitive in localizing the mesial temporal epileptic focus.

## Conclusions

FDG-PET provided the most apparent indications of the side of the epileptic temporal lobe. SPM and ROI analyses were both useful for FDG-PET analysis. ROI analysis is the standard method for determining the side of the epileptic focus in patients with MTLE. On the other hand, SPM analysis is more convenient than ROI analysis and can be used as a substitute for the latter once a system of routine clinical use is established. SPM analysis of FMZ-PET proved to be superior to FDG-PET in the depiction of actual epileptic foci with pathological change.

## References


1. Henry TR, Chugani HT, Abou-Khalil BW, Theodore WH, Swartz BE. Positron emission tomography. In: Engel J Jr, editor. Surgical treatment of the epilepsies. 2nd ed. New York: Raven Press; 1993. p. 211–32.
2. Spencer SS, Bautista RED. Functional neuroimaging in localization of the ictal onset zone. In: Henry TR, Duncan JS, Berkovic SF, editors. Advances in neurology, Vol. 83. Functional imaging in the epilepsies. Philadelphia: Lippincott Williams & Wilkins; 2000. p. 285–96.
3. Henry TR. PET: cerebral blood flow and glucose metabolism-presurgical localization. In: Henry TR, Duncan JS, Berkovic SF, editors. Advances in neurology, Vol. 83. Functional imaging in the epilepsies. Philadelphia: Lippincott Williams & Wilkins; 2000. p. 105–20.
4. Engel J Jr, Henry TR, Risinger MW. The role of positron emission tomography in presurgical evaluation of temporal lobe epilepsy. In: Luders H, editor. Epilepsy surgery. New York: Raven Press; 1991. p. 231–41.
5. Duncan JS, Koepp MJ. PET: central benzodiazepine neuroreceptor mapping in localization-related epilepsies. In: Henry TR, Duncan JS, Berkovic SF, editors. Advances in neurology, Vol. 83. Functional imaging in the epilepsies. Philadelphia: Lippincott Williams & Wilkins; 2000. p. 131–6.
6. Henry TR. Progress in epilepsy research: functional neuroimaging with positron emission tomography. Epilepsia 1996;37:1141–54.
7. Lee DS, Lee JS, Kang KW, Jang MJ, Lee SK, Chung JK, et al. Disparity of perfusion and glucose metabolism of epileptogenic zones in temporal lobe epilepsy demonstrated by SPM/SPAM analysis on $^{15}O$ water PET, [$^{18}$F]FDG-PET, and [$^{99m}$Tc]-HMPAO SPECT. Epilepsia 2001;42:1515–22.
8. Gaillard WD, Fazilat S, White S, Malow B, Sato S, Reeves P, et al. Interictal metabolism and blood flow are uncoupled in temporal lobe cortex of patients with complex partial epilepsy. Neurology 1995;45:1841–7.
9. Leiderman DB, Balish M, Sato S, Kufta C, Reeves P, Gaillard WD, et al. Comparison of PET measurements of cerebral blood flow and glucose metabolism for the localization of human epileptic foci. Epilepsy Res 1992;13:153–7.
10. Ryvlin P, Bouvard S, Le Bars D, De Lamerie G, Gregoire MC, Kahane P, et al. Clinical utility of flumazenil-PET versus [$^{18}$F]fluorodeoxyglucose-PET and MRI in refractory partial epilepsy: a prospective study in 100 patients. Brain 1998;121:2067–81.
11. Savic I, Ingvar M, Stone-Elander S. Comparison of [$^{11}$C]flumazenil and [$^{18}$F]FDG as PET markers of epileptic foci. J Neurol Neurosurg Psychiatry 1993;56:615–21.
12. Engel J Jr, Van Ness PC, Rasmussen TB, Ojemann LM. Outcome with respect to epileptic seizure. In: Engel J Jr, editor. Surgical treatment of the epilepsies. 2nd ed. New York: Raven Press; 1993. p. 609–21.
13. Ardekani BA, Braun M, Hutton BF, Kanno I, Iida H. A fully automatic multimodality image registration algorithm. J Comput Assist Tomogr 1995;19:615–23.
14. Kuzniecky RI, Cascino GD, Palmini A, Jack CR Jr, Berkovic SF, Jackson GD, et al. Structural neuroimaging. In: Engel J

Jr, editor. Surgical treatment of the epilepsies. 2nd ed. New York: Raven Press; 1993. p. 197–209.
15. Theodore WH. PET: cerebral blood flow and glucose metabolism-pathophysiology and drug effects. In: Henry TR, Duncan JS, Berkovic SF, editors. Advances in neurology, Vol. 83. Functional imaging in the epilepsies. Philadelphia: Lipponcott Williams & Wilkins; 2000. p. 121–30.
16. Takaya S, Hanakawa T, Hashikawa K, Ikeda A, Sawamoto N, Nagamine T, et al. Prefrontal hypofunction in patients with intractable mesial temporal lobe epilepsy. Neurology 2006;67:1674–6.
17. Kim YK, Lee DS, Lee SK, Kim SK, Chung CK, Chang KH, et al. Differential features of metabolic abnormalities between medial and lateral temporal lobe epilepsy: quantitative analysis of $^{18}$F-FDG PET using SPM. J Nucl Med 2003; 44:1006–12.
18. Duarte PS, Zhuang H, Couturier O, Alavi A. Does semiquantitative analysis of FDG-PET have any additional value in the diagnosis of mesial temporal sclerosis? Arq Neuropsiquiatr 2001;59:871–4.
19. Newberg AB, Alavi A, Berlin J, Mozley PD, O'Connor M, Sperling M. Ipsilateral and contralateral thalamic hypometabolism as a predictor of outcome after temporal lobectomy for seizures. J Nucl Med 2000;41:1964–8.
20. Hammers A, Koepp MJ, Labbe C, Brooks DJ, Thom M, Cunningham VJ, et al. Neocortical abnormalities of [$^{11}$C]-flumazenil PET in mesial temporal lobe epilepsy. Neurology 2001;56:897–906.
21. Koepp MJ, Labbe C, Richardson MP, Brooks DJ, Van Paesschen W, Cunningham VJ, et al. Regional hippocampal [$^{11}$C]flumazenil PET in temporal lobe epilepsy with unilateral and bilateral hippocampal sclerosis. Brain 1997;120:1865–76.
22. Koepp MJ, Richardson MP, Labbe C, Brooks DJ, Cunningham VJ, Ashburner J, et al. $^{11}$C-flumazenil PET, volumetric MRI, and quantitative pathology in mesial temporal lobe epilepsy. Neurology 1997;49:764–73.
23. Debets RM, Sadzot B, van Isselt JW, Brekelmans GJ, Meiners LC, van Huffelen AO, et al. Is $^{11}$C-flumazenil PET superior to $^{18}$FDG PET and $^{123}$I-iomazenil SPECT in presurgical evaluation of temporal lobe epilepsy? J Neurol Neurosurg Psychiatry 1997;62:141–50.
24. Meencke HJ, Veith G. Hippocampal sclerosis in epilepsy. In: Luders H, editor. Epilepsy surgery. New York: Raven Press; 1991. p. 705–15.
25. Araujo D, Santos AC, Velasco TR, Wichert-Ana L, Terra-Bustamanate VC, Alexandre V Jr, et al. Volumetric evidence of bilateral damage in unilateral mesial temporal lobe epilepsy. Epilepsia 2006;47:1354–9.